Hindawi Publishing Corporation
Advances in OptoElectronics
Volume 2009, Article ID 278105, 8 pages
doi:10.1155/2009/278105

Research Article

Numerical Simulation of 980 nm-LD-Pumped Yb^{3+}-Er^{3+}-Tm^{3+}-Codoped Fiber Amplifier for 1500 nm and 1600 nm Bands

Chun Jiang

State Key Laboratory of Advanced Optical Communication Systems and Networks, Shanghai Jiao Tong University, Shanghai 200240, China

Correspondence should be addressed to Chun Jiang, cjiang@sjtu.edu.cn

Received 2 March 2009; Accepted 1 May 2009

Recommended by Samir K. Mondal

The theoretical model of Yb^{3+}-Er^{3+}-Tm^{3+}-codoped fiber amplifier pumped by 980 nm laser is proposed, and the rate and power propagation equations are numerically solved to analyze the dependences of the gains at 1500 nm and 1600 nm bands on the activator concentrations, fiber length, pump power, and signal wavelength. The numerical results show that our model is in good agreement with experimental result, and with pump power of 200 mW and fiber length varying from 0.15 to 1.5 m, the gains at the two bands may reach 10.0–20.0 dB when the codoping concentrations of Yb^{3+}, Er^{3+}, and Tm^{3+} are in the ranges $1.0–3.0 \times 10^{25}$, $1.0–3.0 \times 10^{24}$, and $1.0–3.0 \times 10^{24}$ ions/m^3, respectively. The fiber parameters may be optimized to flatten the gain spectra.

1. Introduction

The All-wave fiber without residual OH group is being considered for Coarse Wavelength Division Multiplexing (CWDM) transmission systems and metro area optical networks because it has low-loss bandwidth of about 400 nm (1250–650 nm). WDM technology has been the most important technology of large-capacity optical transmission system, and optical amplifiers are key devices of WDM system. Although Fiber Raman Amplifier (FRA) using split-band and multipump schemes might simultaneously amplify multichannel signal within 130nm bandwidth, it would increase the power penalty of the system and degrade the performance of the system since the introduction of the multiplexing/de-multiplexing caused additional insertion loss [1]. Another kind of FRA could provide distributed amplification within 140 nm bandwidth using pump-signal interleaving method, but its gain spectra had relatively large ripple [1]. Later, a novel multiband FRA was reported theoretically providing flat bandwidth of 200 nm with ripple of 1 dB [2]. However, the FRA requires higher pump power due to its lower pump efficiency. Rare-earth doped fiber amplifiers have higher gain and pump efficiency, and in the past decades the researches on rare-earth-doped fiber amplifiers have been focusing on the singly-doped fiber amplifiers, and all of these amplifiers have their own bandwidths, Er^{3+}-doped fiber amplifier (EDFA) with new parallel configuration [3–5] was reported providing gain bandwidth of more than 100 nm, and Tm^{3+}-doped- and Pr^{3+}-doped fiber amplifiers [6–9] could provide the gains in the ranges 1400–1500 nm, 1280–1340 nm, respectively. Recent reports on emission properties of Er^{3+}-Tm^{3+}-codoped silicate and telluride fibers showed that the combination of the emission at 1500 nm windows with that at 1400 nm windows in a single fiber may generate a large seamless emission spectra with emission width up to 200 nm in the codoped system [10–14]. The upconversion and energy transfer in Yb^{3+}-Er^{3+}-Tm^{3+}- and Er^{3+}-Tm^{3+}-codoped glasses were reported [15]. Energy transfer and upconversion luminescence of Bismuth, Tm^{3+}/Ho^{3+}, Tb^{3+}/Yb^{3+}, Er^{3+}/Tm^{3+}/Yb^{3+}-codoped inorganic materials for display systems were reported [16–30]. In our previous works [31, 32], we presented the numerical model of Er^{3+}-Tm^{3+} codoped telluride fiber amplifier pumped at 800 nm and calculated the dependence of the gains at 1470 nm and 1530 nm bands on the fiber parameters, and analyzed the transmission performance

of the WDM system based on the codoped amplifier. Although the rate equations of Er^{3+}-Tm^{3+}, Er^{3+}-Yb^{3+}-Tm^{3+}-codoped fluoride glasses was reported in [15], the equations just considered the upconversion of infrared to visible light for display system, did not consider the spontaneous and stimulated emissions of 1470 nm, 1530 nm, and 1630 nm bands. Other references on this codoped system just concentrated on the spectral properties. Owing to importance of the double and multidoped systems for broadband amplification of telecommunication wavelength, a theoretical model will be desirable for designing and optimizing the codoped broadband amplifiers. In present paper, we propose a new numerical model of Yb^{3+} and Er^{3+} and Tm^{3+} codoped fiber system pumped by 980 nm laser for amplification of the signal at 1470, 1530, and 1630 nm bands. This model considers the excited state absorption and upconversion of Er^{3+} and Tm^{3+} ions and cross-relaxation of Tm^{3+}-Er^{3+}. The dependence of the gain spectra covering 1500 and 1600 nm bands on codoping concentrations, fiber length, and pump power is calculated and analyzed.

2. Theoretical Model

Figure 1 shows the schematic of the energy levels and electron transitions and energy transfer process of an Er^{3+}-Tm^{3+}-Yb^{3+} codoped telluride glass system pumped by 980 nm. With the excitation of 980 nm pump, the electrons of Yb^{3+} ions are excited from the ground state ($^2F_{7/2}$) to the excited state ($^2F_{5/2}$) and the energy at the $^2F_{5/2}$ level transfers to the $^4I_{11/2}$ level of Er^{3+} due to matching energy gap between the two levels, meanwhile, the energy at the level also can transfer to the $^3F_4$ level of Tm^{3+} ion through multiphonon process. With the excitation, moreover, the electrons of Er^{3+} ions are excited from the ground state $^4I_{15/2}$ to the excited state $^4I_{11/2}$, then nonradiately relax to the $^4I_{13/2}$ level through multiphonon process, and transit from the level to the ground state ($^4I_{15/2}$ level), emitting photons at 1500 nm band. In addition, the electrons at $^4I_{11/2}$ level of Er^{3+} ions can be excited to the $^4F_{7/2}$ level due to excited state absorption (ESA), and the electrons at the $^4F_{7/2}$ level transit to the ground state with emission of red photon. On the other hand, energy transfer also can take place between Er^{3+}-Tm^{3+} and Yb^{3+}-Tm^{3+} via cross-relaxation process. The energy at the $^4I_{13/2}$ level of Er^{3+} ions and the $^2F_{5/2}$ level of Yb^{3+} ions can transfer to the $^3F_4$, $^3F_2$ levels of Tm^{3+} ions via the electron transition from the $^3F_4$ level to $^3F_2$ level of Tm^{3+} at which the electron nonradiately relax to $^3H_4$ level from which is excited to the $^1G_4$ level via another cross-relaxation process. Electron at the $^1G_4$ level transit to the $^3F_2$, $^3F_4$, and $^3H_6$ levels with emission of lights at 1630, 650, and 476 nm bands, respectively. The electron at $^3F_2$ level nonradiately relaxes to $^3H_4$ level and then transites to the $^3F_4$ level with emission of light at 1470 nm band. The electrons at $^3F_4$ level transit to ground state ($^3H_6$), emitting the light at 1680 nm band.

According to Figure 1, a rate equation group can be written as follows:

$$
\begin{aligned}
\frac{\partial N_1}{\partial t} &= (W_{12} - W_{13})N_1 + (W_{21} + A_{21})N_2 + W_{ET28}N_2N_7 \\
&\quad + W_{41}N_4 - W_{ET63}N_6N_1, \\
\frac{\partial N_2}{\partial t} &= W_{12}N_1 - (W_{21} + A_{21})N_2 + A_{32}N_3 - W_{ET28}N_2N_7, \\
\frac{\partial N_3}{\partial t} &= -A_{32}N_3 + W_{ET63}N_6N_1 - W_{34}N_3 \\
&\quad + W_{13}N_1 - W_{ET64}N_6N_3, \\
\frac{\partial N_4}{\partial t} &= W_{34}N_3 + W_{ET64}N_6N_3 - W_{41}N_4, \\
\frac{\partial N_6}{\partial t} &= W_{56}N_5 - W_{ET63}N_6N_1 - W_{ET64}N_6N_3 - W_{ET68}N_6N_7 \\
&\quad - W_{ET6-10}N_6N_8 - W_{ET6-11}N_6N_9 - A_{65}N_6, \\
\frac{\partial N_7}{\partial t} &= A_{87}N_8 + W_{97}N_9 - W_{ET68}N_6N_7 \\
&\quad - W_{ET28}N_2N_7 + A_{11-7}N_{11}, \\
\frac{\partial N_8}{\partial t} &= -A_{87}N_8 + W_{ET68}N_6N_7 + W_{ET28}N_2N_7 \\
&\quad - (W_{8-10} + W_{ET6-10}N_6)N_8 + A_{11-8}N_{11}, \\
\frac{\partial N_9}{\partial t} &= A_{10-9}N_{10} - W_{ET6-11}N_6N_9 - W_{97}N_9, \\
\frac{\partial N_{10}}{\partial t} &= -A_{10-9}N_{10} + (W_{8-10} + W_{ET6-10}N_6)N_8 \\
&\quad - W_{10-11}N_{10} + W_{11-10}N_{11} + A_{11-10}N_{11}, \\
\frac{\partial N_{11}}{\partial t} &= W_{10-11}N_{10} - A_{11-10}N_{11} - W_{11-10}N_{11} \\
&\quad + W_{ET6-11}N_6N_9 - (A_{11-8} + A_{11-7})N_{11},
\end{aligned}
\tag{1}
$$

where N_1, N_2, N_3, N_4 are the population densities of Er^{3+} at energy levels 1, 2, 3, and 4, and N_5 and N_6 are the population densities of Yb^{3+} at energy levels 1 and 2 and N_7, N_8, N_9, N_{10}, N_{11} are the population densities of Tm^{3+} at energy levels 1, 2, 3, 4, and 5, W_{13}, W_{56}, and W_{79} are the pump transition rates, W_{ij} $(i, j = 1 \sim 11)$ is the transition rate between energy levels i and j of the activating ions (Er^{3+}, Yb^{3+}, Tm^{3+}), and W_{ETij} $(i, j = 1 \sim 11)$ is the transfer rate between energy level i and j. A_{ij} $(i, j = 1 \sim 11)$ is the spontaneous transition rate between energy level i and j. N_{er}, N_{yb}, N_{tm} are total

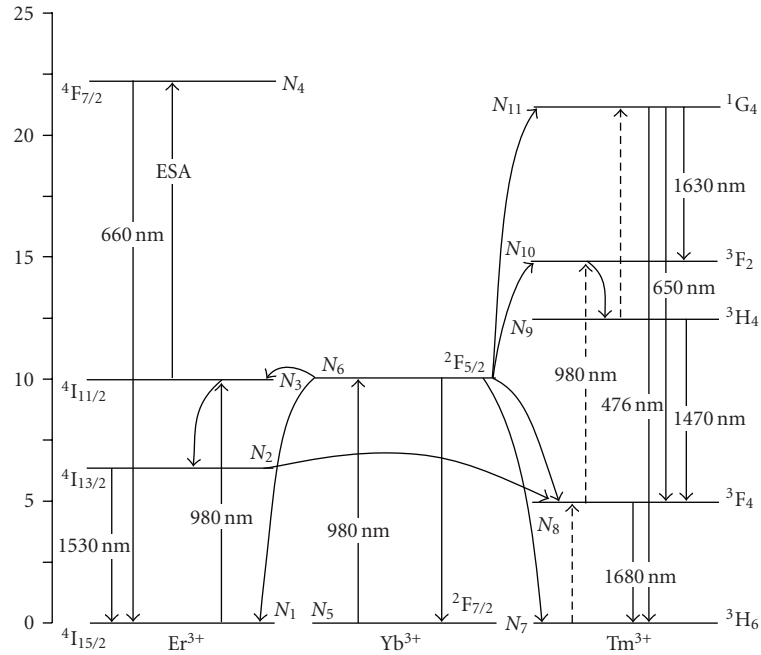

Figure 1: The schematic of energy level and transition configuration and energy transfer process of Yb^{3+}, Er^{3+} and Tm^{3+} codoped telluride fiber system pumped with 980 nm LD.

concentrations of Er^{3+}, Yb^{3+}, and Tm^{3+} ions, respectively. The transition rates are as follows:

$$W_{13} = \frac{\sigma_{13}P_P}{h\nu_P A_{\text{eff}}}, \qquad W_{56} = \frac{\sigma_{56}P_P}{h\nu_P A_{\text{eff}}}, \qquad W_{8-10} = \frac{\sigma_{8-10}P_P}{h\nu_P A_{\text{eff}}},$$
$$W_{ij} = \frac{\sigma_{ij}P_s}{h\nu_s A_{\text{eff}}}, \tag{2}$$

where $\sigma_{13}, \sigma_{56}, \sigma_{8-10}$ are the pump absorption cross-section, σ_{ij} is the absorption and emission cross-sections of the transitions between levels i and j. A_{eff} is the effective cross-section area of the fiber.

The power propagations of the pump and signal and amplified spontaneous emission (ASE) along the fiber are described by differential equation group (3), where P_P is the pump power at 980 nm, P_{S1}, P_{S2}, and P_{S3} are the power of the signals at 1470 nm, 1530 nm, and 1630 nm, respectively. P_{ASE1}, P_{ASE2}, P_{ASE3} are the ASE powers in the 1470, 1530, and 1630 bands, and Γ_1470, Γ_1530, Γ_1630, and $\Gamma\_\lambda_{\text{ASE}}$ are overlap factors at 1470 nm, 1530 nm, and 1630 nm, and ASE wavelength, respectively, and υ_s, υ_p are signal and pump frequencies, respectively. h and $\alpha(\nu)$ are Plank constant, the frequency-independent back-ground loss of the active fiber, respectively,

$$\begin{aligned}
\frac{dP_{S1}}{dz} &= \Gamma_{1470}(N_9\sigma_{98} - N_8\sigma_{89})P_{S1} - \alpha_{1470}P_{S1},\\
\frac{dP_{S2}}{dz} &= \Gamma_{1530}(N_2\sigma_{21} - N_1\sigma_{12})P_{S2} - \alpha_{1530}P_{S2},\\
\frac{dP_{S3}}{dz} &= \Gamma_{1630}(N_{11}\sigma_{11-10} - N_{10}\sigma_{10-11} + N_8\sigma_{87})P_{S3}\\
&\quad - N_7\sigma_{78}P_{S3} - \alpha_{1630}P_{S3},\\
\frac{dP_P}{dz} &= -\Gamma_{980}[(N_1\sigma_{13} - N_3\sigma_{31}) + (N_5\sigma_{56} - N_6\sigma_{65})\\
&\quad + (N_{10}\sigma_{10-8} - N_8\sigma_{8-10})]P_P - \alpha_{980}P_P,\\
\frac{\partial P_{\text{ASE1}}}{\partial z} &= \Gamma(\lambda_{\text{ASE1}})(\sigma_{98}N_9 - \sigma_{89}N_8)P_{\text{ASE1}}\\
&\quad + \Gamma(\lambda_{\text{ASE1}})2h\Delta_{\text{ASE1}}\upsilon\sigma_{98}N_9 - \alpha P_{\text{ASE1}},\\
\frac{\partial P_{\text{ASE2}}}{\partial z} &= \Gamma(\lambda_{\text{ASE2}})(\sigma_{21}N_2 - \sigma_{12}N_1)P_{\text{ASE2}}\\
&\quad + \Gamma(\lambda_{\text{ASE2}})2h\Delta_{\text{ASE2}}\upsilon\sigma_{21}N_2 - \alpha P_{\text{ASE2}},\\
\frac{\partial P_{\text{ASE3}}}{\partial z} &= \Gamma(\lambda_{\text{ASE3}})(\sigma_{11-10}N_{11} - \sigma_{10-11}N_{10} + \sigma_{8-7}N_8)P_{\text{ASE3}}\\
&\quad - \sigma_{7-8}N_7P_{\text{ASE3}}\\
&\quad + \Gamma(\lambda_{\text{ASE3}})2h\Delta\upsilon_{\text{ASE3}}(N_8\sigma_{8-7} + \sigma_{11-10}N_{11}) - \alpha P_{\text{ASE3}}.
\end{aligned} \tag{3}$$

The above power propagation equation group forms a system of coupled differential equations, which will be solved by numerical integration using Newton and Lung-Kutta methods along the active fiber. It was assumed that the energy transfer rates $W_{\text{ET\_YE}}$, $W_{\text{ET\_YT}}$, $W_{\text{ET\_ET}}$ were

increasing functions of $N_{\mathrm{Yb}}, N_{\mathrm{Er}}$, and N_{Tm} [33–35], and expressed in the following equation:

$$W_{\mathrm{ET\_YE}} = 1.0\times10^{-22} + 4.0\times10^{-49}\left[(N_{\mathrm{Yb}}N_{\mathrm{Er}})^{1/2} - 1.0\times10^{25}\right],$$
$$W_{\mathrm{ET\_ET}} = 1.0\times10^{-22} + 4.0\times10^{-49}\left[(N_{\mathrm{Er}}N_{\mathrm{Tm}})^{1/2} - 1.0\times10^{25}\right],$$
$$W_{\mathrm{ET\_YT}} = 1.0\times10^{-22} + 4.0\times10^{-49}\left[(N_{\mathrm{Yb}}N_{\mathrm{Tm}})^{1/2} - 1.0\times10^{25}\right]. \quad (4)$$

3. Results and Discussion

3.1. Comparison with Experimental Results. The spontaneous spectra of Yb^{3+}-Er^{3+}-Tm^{3+}-telluride glasses excited near 980 nm were measured with two emission peaks [36]. The ratio of Yb^{3+}, Er^{3+}, Tm^{3+} ion concentrations in the glass samples with thickness of 1.5 mm was 10 : 1 : 1 and 10 : 1 : 2, two stronger emission peaks were observed in the samples. To verify our theoretical model, same parameters as the sample are used to calculated the luminescence intensity, and calculated emission spectra and measured emission spectra from the reference are normalized and plotted in Figure 2 where solid line represent calculated spectra, and the measured spectra from [36] are denoted using circle, it is shown that calculated spectra are in good agreement with the measured, verifying feasibility of our model.

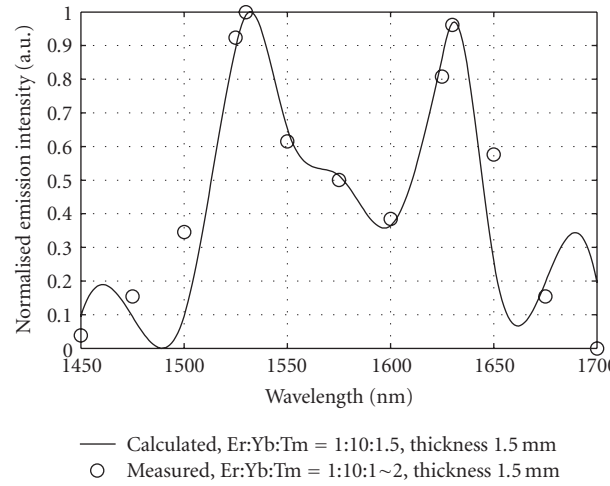

Figure 2: Comparison of calculated normalized emission intensity of Yb^{3+}-Er^{3+}-Tm^{3+} codoped telluride glass excited at 980 nm with measured normalized emission intensity, the measured results from [36].

3.2. Activator Concentration Dependence. The gain spectra is calculated by solving numerically the equation groups (1)–(3). Table 1 is the spectroscopic parameters for the Er^{3+}-doped and Tm^{3+}-doped telluride glass fiber for this calculation, the parameters of Yb^{3+} is from [36], the core diameter of fiber is 5 μm and numerical aperture is 0.21, and the input power of signal is −30 dBm.

Dependence of the gain spectra in the range 1450–1700 nm on Er^{3+} concentration is shown Figure 3(a). With Yb^{3+} concentration of 20.0×10^{24} ions/m^3 and Tm^{3+} concentration of 1.0×10^{24} ions/m and fixed fiber length at 1.5 m and when the Er^{3+} concentration increases from 1.0×10^{24} to 3.0×10^{24} ions/m^3, the gains at the range 1510–1630-nm increase, where the gain at the 1530 nm increases from 10.0 to 21.0 dB, the gains beyond 1630 nm keep constant. Figure 3(b) demonstrates variation of the gain spectra with Tm^{3+} concentration. With Yb^{3+} concentration of 20.0×10^{24} ions/m^3 and Er^{3+} concentration of 1.0×10^{24} ions/m and fixed fiber length at 1.5 m and when the Tm^{3+} concentration increases from 1.0×10^{24} to 3.0×10^{24} ions/m^3, the gains at the range 1510–1650 nm increase, where the gain at the 1530 nm increases from 10.5 to 17.8 dB, and the gain at 1630 nm increases from 7.0 to 9.8-dB . Effect of Yb^{3+} concentration on the gain spectra is shown Figure 3(c). With both Er^{3+} and Tm^{3+} concentrations of 1.0×10^{24} ions/m^3 and fixed fiber length at 1.5 m and when the Yb^{3+} concentration increases from 10.0×10^{24} to 30.0×10^{24} ions/m^3, the gains at the range 1510–1610 nm decrease, and the gain at the 1610–1650 nm increase.

3.3. Fiber Length Effect. Effect of fiber length on the gain spectra is shown Figure 4. With Yb^{3+} concentration of 20.0×10^{24} ions/m^3, Er^{3+} concentration of 1.0×10^{24} ions/m and Tm^{3+} concentration of 3.0×10^{24} ions/m, when fiber length increases from 0.15 to 0.25 m, the gains at the range 1500–1630 nm increase, where the gain at the 1530 nm increases from 12.5 to 24.5 dB, and the gains at 1630 nm decreases from 10.0 to 5.0 dB .

3.4. Variation with Pump Power. Variation of the gain spectra with pump power is shown in Figure 5. With Yb^{3+} concentration of 20.0×10^{24} ions/m^3, Er^{3+} concentration of 1.0×10^{24} ions/m and Tm^{3+} concentration of 3.0×10^{24} ions/m and fiber length of 1.5 m, when pump power increases from 100 to 300 mW, the gains at the range 1500–1610 nm increase, where the gain at the 1530 nm increases from −14.0 to 27.0 dB, and the gain at 1630 nm decreases from 10.0 to −1.0 dB.

4. Discussion

In above results, one notes that with increasing Yb^{3+} concentration from 1.0×10^{25} to 3.0×10^{25} ions/m^3, the gains at the range 1510–1610 nm decrease, and the gains at the 1610–1650 nm increase, showing different Yb^{3+} ion concentration dependences of gain spectra in different wave band. These different dependences, we think, may be explained using energy transfer from Yb^{3+} to Er^{3+} and from Yb^{3+} to Tm^{3+} ions. When Yb^{3+} ion concentration increases, the pump absorption induced by Yb^{3+} increases and the pump absorption by Er^{3+} decreases, this leads to (1) increased energy transfer from Yb^{3+} to Tm^{3+} ions

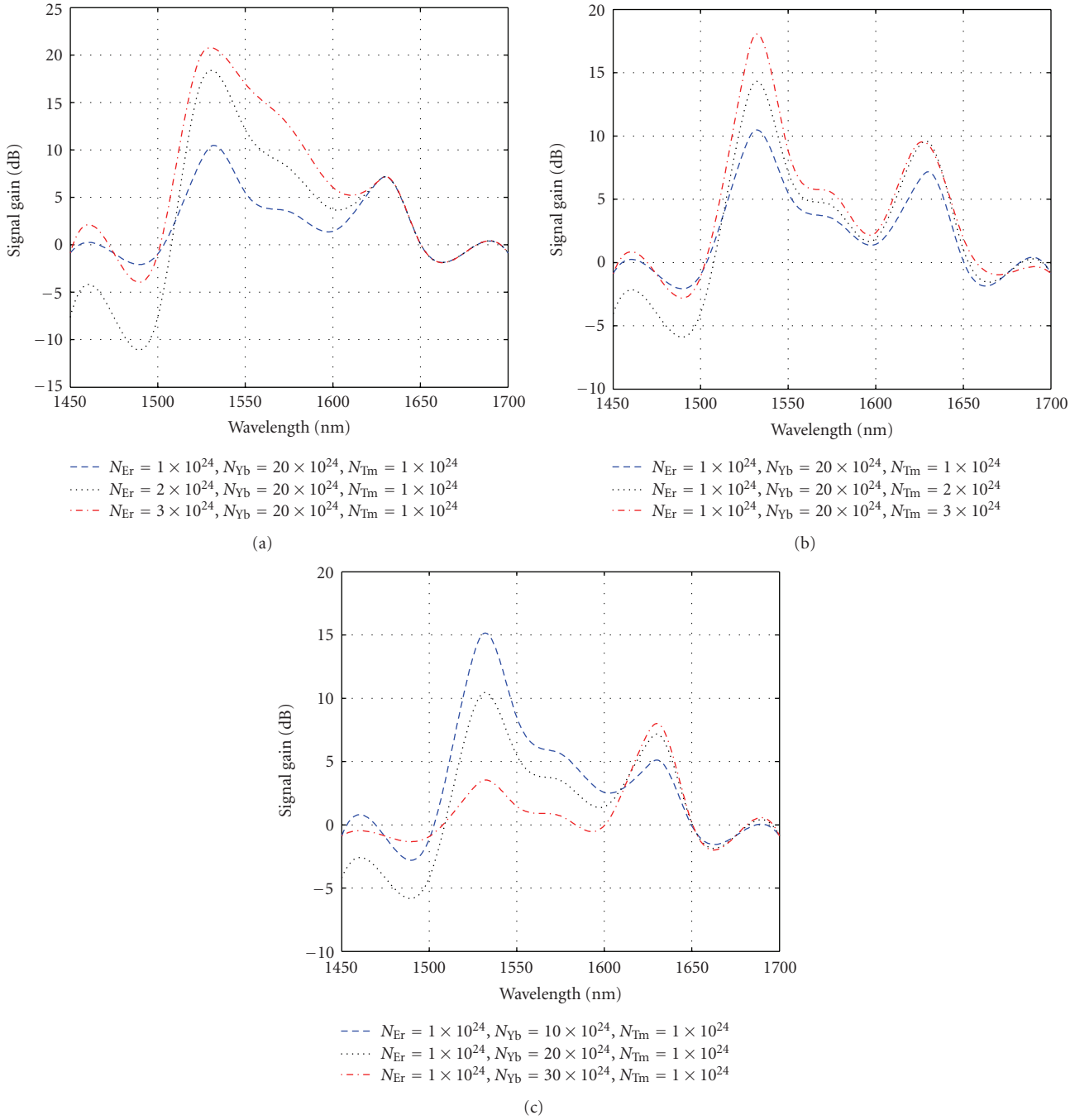

Figure 3: Variation of the gain spectra with Er^{3+} ion concentration (a), Tm^{3+} ion concentration (b), and Yb^{3+} ion concentration (c). Fiber length, pump power, and input signal power are 1.5 m, 980 nm, 200 mW, −30 dBm, respectively.

and increased population inversion between $^3H_4$ and $^3F_4$ of Tm^{3+} ions and thus increased gain at 1630 nm band, and (2) increased energy transfer from Yb^{3+} to Er^{3+} ions, but reduced pump absorption of Er^{3+} probably dominates over the increased energy transfer, thus results in reduced population inversion between the $^4I_{13/2}$ and $^4I_{15/2}$ levels of Er^{3+} and decreased gain at 1530 nm band.

Meanwhile, one also notes that with increasing pump power, the increasing of the gain spectra in 1500–1610 nm and the decreasing of the gain spectra in 1610–1650 nm show different pump-power effect on the gain spectra in different wave band. These different effects may be explained using energy transfer from Yb^{3+} to Er^{3+} and from Yb^{3+} to Tm^{3+} ions. With the power increasing, the pump absorptions caused by Yb^{3+} and Er^{3+} and Tm^{3+} increase simultaneously, this leads to increased population inversion between the $^4I_{13/2}$ and $^4I_{15/2}$ levels of Er^{3+} and thus increased gain at 1500–1610 nm band. The efficiency of the increasing of

Table 1: Spectroscopic parameters of Er^{3+}-doped and Tm^{3+} doped telluride fiber for numerical calculation.

Parameter	Symbol	Value	Unit	Remarks
Core diameter	$2r$	5.0	μm	
Background loss	α	0.1	dB/m	
Spontaneous emission rate (Er^{3+})	A_{10}	172.4	1/s	[37]
	A_{40}	1804.3	1/s	
	A_{21}	1000	1/s	
	A_{32}	51000	1/s	
	A_{54}	51000	1/s	
	A_{65}	51000	1/s	
Spontaneous emission rate (Tm^{3+})	a_{21}	311	1/s	[37]
	a_{32}	131	1/s	
Energy transfer rate	W_{ET1}	140	1/s	[38]
	W_{ET3}	985	1/s	
Transition rate of ASE	A_{87}	400	1/s	[37]
	A_{41}	1804.3	1/s	
Pump absorption cross section	σ_{p1}	1.0×10^{-25}	m^2	[38]
	σ_{p2}	1.0×10^{-26}	m^2	
	σ_{p3}	1.0×10^{-25}	m^2	
Stimulated emission cross section (Er^{3+})	σ_{21}	8.6×10^{-25}	m^2	[38]
	σ_{12}	8.5×10^{-25}	m^2	
Pump emission cross section (Er^{3+})	σ_{31}	1.0×10^{-26}	m^2	[38]
Stimulated emission cross section (Tm^{3+})	σ_{97}	4.5×10^{-25}	m^2	[38]
	σ_{79}	4.5×10^{-25}	m^2	
	σ_{87}	8.6×10^{-25}	m^2	
	σ_{78}	8.6×10^{-25}	m^2	

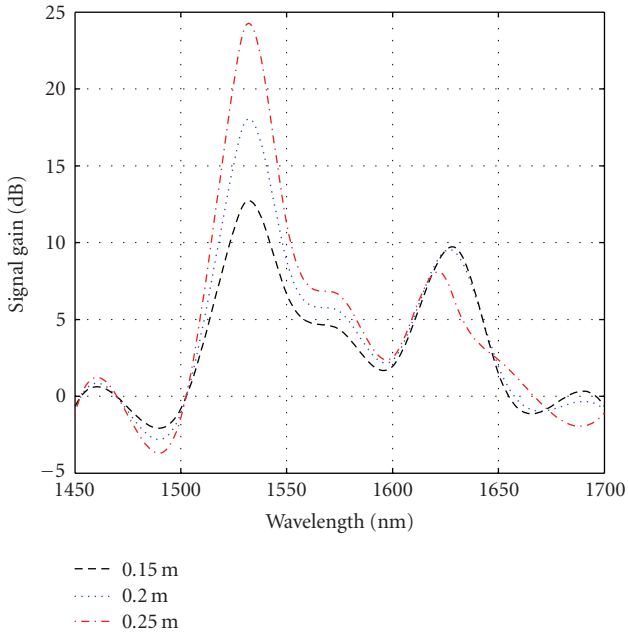

Figure 4: Dependence of the gain spectra with fiber length, the concentrations of Yb^{3+}, Er^{3+}, Yb^{3+}, ion are 20.0×10^{24}, 1.0×10^{24}, 3.0×10^{24} ions/m^3, respectively, and pump power, and input signal power are 200 mW, −30 dBm, respectively.

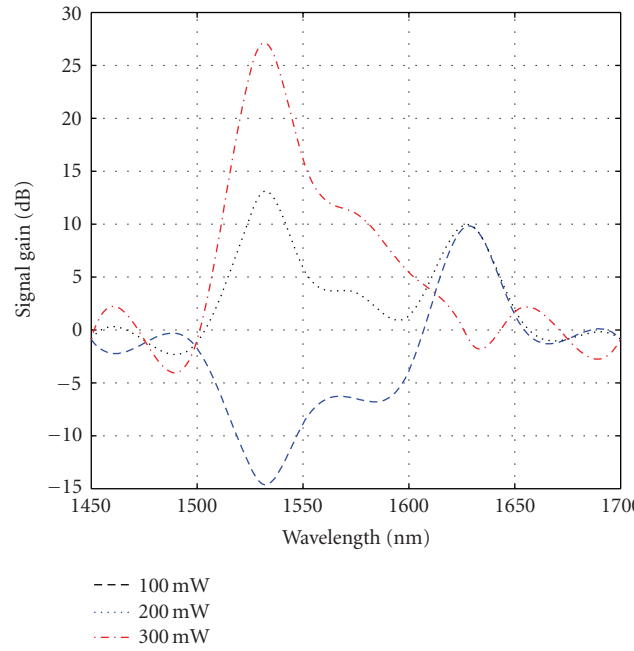

Figure 5: Effect of pump power on gain spectra. Concentrations of Yb^{3+}, Er^{3+}, Yb^{3+} ion are 20.0×10^{24}, 1.0×10^{24}, 3.0×10^{24} ions/m^3, respectively. Fiber length, input signal power are 1.5 m, −30 dBm, respectively.

pump absorption caused by Tm^{3+} is less than that caused by Er^{3+} because the former depends highly on the population number of the $^3F_4$ level of Tm^{3+} ions coming from energy transfer from Yb^{3+} and Er^{3+} to Tm^{3+}. Moreover, increasing pump absorption can increase the population of the $^3F_2$ level of Tm^{3+} ions, hence the population inversion between $^1G_4$ and $^3F_2$ of Tm^{3+} ions and the gain at 1610–1650 nm band is reduced if the lifetime at $^1G_4$ level is shorter than that at $^3F_2$ level.

It is shown from Figures 3, 4, and 5 that two weak peaks in the gain spectra appear at 1470 nm and 1680 nm, resulting separately from the transitions from the $^3H_4$ to $^3F_4$ levels and from $^3H_4$ to $^3H_6$ levels of Tm^{3+} ions. If both pumps at 800 nm and 980 nm are used, the gain spectra covering 1470 nm, 1530 nm, 1630 nm, 1680 nm bands may appear, further study is needed to optimize the fiber parameter and pump configuration to reduce the ripple of the gain spectra.

5. Conclusions

In conclusion, we present the numerical model of Yb^{3+}-Er^{3+}-Tm^{3+}-codoped fiber amplifier pumped by 980 nm laser and analyzed the dependences of the gains at 1530 nm and 1630 nm on the activator codoping concentrations, fiber length, signal wavelength. The numerical results showed that our model was in good agreement with experimental result, and with pump power of 200 mW and fiber length varying from 0.15 to 1.5-m, the gains at the two bands could reach 10.0–20.0 dB when the codoping concentrations of Yb^{3+}, Er^{3+}, and Tm^{3+} were in the ranges $1.0–3.0 \times 10^{25}$, $1.0–3.0 \times 10^{24}$, $1.0–3.0 \times 10^{24}$ ions/m^3, respectively. Two weak peaks in the gain spectra appeared at 1470 nm and 1680 nm, resulting separately from the transitions from the $^3H_4$ to $^3F_4$ levels and from $^3H_4$ to $^3H_6$ levels of Tm^{3+} ions. If both pumps at 800 nm and 980 nm will be used, the gain spectra covering 1470 nm, 1530 nm, 1630 nm, 1680 nm bands may appear. The optimization of the fiber parameter and two-pump configuration will be desirable for reducing the ripple of the gain spectra.

Acknowledgments

This work is supported in part by National Natural Science Foundation of China (Grant No.60377023 and No.60672017) and Program for New Century Excellent Talents in University and Shanghai Optical Science and Technology (No.05DZ22 0-09) and sponsored by Shanghai Pujiang Program. Thank is given to Mr. Jianda Liu for his numerical analysis code when he was with SJTU.

References

[1] T. Naito, T. Tanaka, K. Torii, N. Shimojoh, H. Nakamoto, and M. Suyama, "A broadband distributed Raman amplifier for bandwidths beyond 100 nm," in *Proceedings of the Optical Fiber Communication Conference and Exhibit (OFC '02)*, vol. 70, pp. 116–117, Anaheim, Calif, USA, March 2002.

[2] C. Jiang and W. Hu, "Multiband-fiber Raman amplifier," in *Proceedings of the 9th Opto-Electronics and Communications Conference & 3rd International Conference on Optical Internet*, pp. 314–315, Pacifica Yokohama, Japan, July 2004.

[3] C. R. Giles and E. Desurvire, "Modeling erbium-doped fiber amplifiers," *Journal of Lightwave Technology*, vol. 9, no. 2, pp. 271–283, 1991.

[4] C.-H. Yeh, C.-C. Lee, and S. Chi, "120-nm bandwidth erbium-doped fiber amplifier in parallel configuration," *IEEE Photonics Technology Letters*, vol. 16, no. 7, pp. 1637–1639, 2004.

[5] Y. B. Lu, P. L. Chu, A. Alphones, and P. Shum, "A 105-nm ultrawide-band gain-flattened amplifier combining C- and L-band dual-core EDFAs in a parallel configuration," *IEEE Photonics Technology Letters*, vol. 16, no. 7, pp. 1640–1642, 2004.

[6] E. R. M. Taylor, L. N. Ng, J. Nilsson, et al., "Thulium-doped tellurite fiber amplifier," *IEEE Photonics Technology Letters*, vol. 16, no. 3, pp. 777–779, 2004.

[7] R. M. Percival and J. R. Williams, "Highly efficient 1.064 μm upconversion pumped 1.47 μm thulium doped fluoride fibre amplifier," *Electronics Letters*, vol. 30, no. 20, pp. 1684–1685, 1994.

[8] T. Kasamatsu, Y. Yano, and T. Ono, "1.49-μm-band gain-shifted thulium-doped fiber amplifier for WDM transmission systems," *Journal of Lightwave Technology*, vol. 20, no. 10, pp. 1826–1838, 2002.

[9] Y. Ohishi, T. Kanamori, T. Nishi, et al., "Concentration effect on gain of Pr^{3+} -doped fluoride fiber amplifier for 1.3 μm," *IEEE Photonics Technology Letters*, vol. 4, no. 12, pp. 1338–1340, 1992.

[10] L. Huang, A. Jha, S. Shen, and X. Liu, "Broadband emission in Er^{3+}-Tm^{3+} codoped tellurite fibre," *Optics Express*, vol. 12, no. 11, pp. 2429–2434, 2004.

[11] H. Jeong, K. Oh, S. R. Han, and T. F. Morse, "Characterization of broadband amplified spontaneous emission from an Er^{3+} - Tm^{3+} co-doped silica fiber," *Chemical Physics Letters*, vol. 367, no. 3-4, pp. 507–511, 2003.

[12] X.-S. Wang, Q.-H. Nie, L.-R. Liu, et al., "Improved fluorescence from $Tm^{3+}/Er^{3+}/Ce^{3+}$ triply doped bismuth-silicate glasses for S+C-bands amplifiers," *Chinese Physics Letters*, vol. 23, no. 9, pp. 2553–2556, 2006.

[13] Z. Xiao, R. Serna, and C. N. Afonso, "Broadband emission in Er-Tm codoped Al_2O_3 films: the role of energy transfer from Er to Tm," *Journal of Applied Physics*, vol. 101, no. 3, Article ID 033112, 2007.

[14] D. Chen, Y. Wang, F. Bao, and Y. Yu, "Broadband near-infrared emission from Tm^{3+}/Er^{3+} co-doped nanostructured glass ceramics," *Journal of Applied Physics*, vol. 101, no. 11, Article ID 113511, 2007.

[15] D. C. Yeh, R. R. Petrin, W. A. Sibley, V. Madigou, J. L. Adam, and M. J. Suscavage, "Energy transfer between Er^{3+} and Tm^{3+} ions in a barium fluoridethorium fluoride glass," *Physical Review B*, vol. 39, no. 1, pp. 80–90, 1989.

[16] S. Tanabe, K. Suzuki, N. Soga, and T. Hanada, "Mechanisms and concentration dependence of Tm^{3+} blue and Er^{3+} green up-conversion in codoped glasses by red-laser pumping," *Journal of Luminescence*, vol. 65, no. 5, pp. 247–255, 1995.

[17] X. Zou, A. Shikida, H. Yanagita, and H. Toratani, "Mechanisms of upconversion fluorescences in Er^{3+}, Tm^{3+} codoped fluorozircoaluminate glasses," *Journal of Non-Crystalline Solids*, vol. 181, no. 1-2, pp. 100–109, 1995.

[18] W. Lozano B., C. B. de Araújo, and Y. Messaddeq, "Enhanced frequency upconversion in Er^{3+} doped fluoroindate glass due to energy transfer from Tm^{3+}," *Journal of Non-Crystalline Solids*, vol. 311, no. 3, pp. 318–322, 2002.

[19] M. Liao, L. Hu, Y. Fang, et al., "Upconversion properties of Er^{3+}, Yb^{3+} and Tm^{3+} codoped fluorophosphate glasses," *Spectrochimica Acta Part A*, vol. 68, no. 3, pp. 531–535, 2007.

[20] Z. Yang and Z. Jiang, "Frequency upconversion emissions in layered lead-germanate-tellurite glasses for three-color display," *Journal of Non-Crystalline Solids*, vol. 351, no. 30-32, pp. 2576–2580, 2005.

[21] S. Xu, H. Ma, D. Fang, Z. Zhang, and Z. Jiang, "$Tm^{3+}/Er^{3+}/Yb^{3+}$-codoped oxyhalide tellurite glasses as materials for three-dimensional display," *Materials Letters*, vol. 59, no. 24-25, pp. 3066–3068, 2005.

[22] V. K. Tikhomirov, K. Driesen, C. Görller-Walrand, and M. Mortier, "Mid-infrared emission in Yb^{3+}-Er^{3+}-Tm^{3+} co-doped oxyfluoride glass-ceramics," *Materials Science and Engineering: B*, vol. 146, no. 1–3, pp. 66–68, 2008.

[23] Z. Duan, J. Zhang, W. Xiang, H. Sun, and L. Hu, "Multicolor upconversion of $Er^{3+}/Tm^{3+}/Yb^{3+}$ doped oxyfluoride glass ceramics," *Materials Letters*, vol. 61, no. 11-12, pp. 2200–2203, 2007.

[24] V. K. Tikhomirov, K. Driesen, C. Görller-Walrand, and M. Mortier, "Broadband telecommunication wavelength emission in Yb^{3+}-Er^{3+}-Tm^{3+} co-doped nano-glass-ceramics," *Optics Express*, vol. 15, no. 15, pp. 9535–9540, 2007.

[25] C. Cao, W. Qin, J. Zhang, et al., "Up-conversion white light of $Tm^{3+}/Er^{3+}/Yb^{3+}$ tri-doped CaF_2 phosphors," *Optics Communications*, vol. 281, no. 6, pp. 1716–1719, 2008.

[26] S. Ye, B. Zhu, J. Chen, J. Luo, and J. R. Qiu, "Infrared quantum cutting in Tb^{3+}, Yb^{3+} codoped transparent glass ceramics containing CaF_2 nanocrystals," *Applied Physics Letters*, vol. 92, no. 14, Article ID 141112, 2008.

[27] G. Lakshminarayana, R. Vidya Sagar, and S. Buddhudu, "NIR luminescence from Er^{3+}/Yb^{3+}, Tm^{3+}/Yb^{3+}, Er^{3+}/Tm^{3+} and Nd^{3+} ions-doped zincborotellurite glasses for optical amplification," *Journal of Luminescence*, vol. 128, no. 4, pp. 690–695, 2008.

[28] S. Shen, B. Richards, and A. Jha, "Enhancement in pump inversion efficiency at 980 nm in Er^{3+}, Er^{3+}/Eu^{3+} and Er^{3+}/Ce^{3+} doped tellurite glass fibers," *Optics Express*, vol. 14, no. 12, pp. 5050–5054, 2006.

[29] B. Richards, S. Shen, A. Jha, Y. Tsang, and D. Binks, "Infrared emission and energy transfer in Tm^{3+}, Tm^{3+}-Ho^{3+} and Tm^{3+}-Yb^{3+}-doped tellurite fibre," *Optics Express*, vol. 15, no. 11, pp. 6546–6551, 2007.

[30] S. Zhou, N. Jiang, B. Zhu, et al., "Multifunctional bismuth-doped nanoporous silica glass: from blue-green, orange, red, and white light sources to ultra-broadband infrared amplifiers," *Advanced Functional Materials*, vol. 18, no. 9, pp. 1407–1413, 2008.

[31] L. Jin, D. Ma, Y. Ding, and C. Jiang, "Theoretical analysis of gain characteristics of Er^{3+}-Tm^{3+}-codoped tellurite fiber amplifier," *IEEE Photonics Technology Letters*, vol. 18, no. 3, pp. 460–462, 2006.

[32] W. Xu, Y. M. Lin, and C. Jiang, "Er^{3+}- Tm^{3+}-codoped tellurite fiber amplifiers for WDM systems: a theoretical analysis of BER and bandwidth," *IEEE Journal of Quantum Electronics*, vol. 45, no. 1, pp. 3–9, 2009.

[33] F. Di Pasquale and M. Federighi, "Improved gain characteristics in high-concentration Er^{3+}/Yb^{3+} codoped glass waveguide amplifiers," *IEEE Journal of Quantum Electronics*, vol. 30, no. 9, pp. 2127–2131, 1994.

[34] M. Karásek, "Optimum design of Er^{3+}-Yb^{3+} codoped fibers for large-signal high-pump-power applications," *IEEE Journal of Quantum Electronics*, vol. 33, no. 10, pp. 1699–1705, 1997.

[35] E. Yahel and A. A. Hardy, "Modeling and optimization of short Er^{3+}-Yb^{3+} codoped fiber lasers," *IEEE Journal of Quantum Electronics*, vol. 39, no. 11, pp. 1444–1451, 2003.

[36] S.-X. Dai, J.-H. Yang, S.-Q. Xu, et al., "Multi-rare-earth ions codoped tellurite glasses for potential dual wavelength fibre-optic amplifiers," *Chinese Physics Letters*, vol. 20, no. 1, pp. 130–132, 2003.

[37] F. X. Gan, *Optical and Spectroscopic Properties of Glasses*, Shanghai Science and Technology Press, Shanghai, China, 1992.

[38] S. Shen, A. Jha, X. Liu, et al., "Tellurite glasses for broadband amplifiers and integrated optics," *Journal of the American Ceramic Society*, vol. 85, no. 6, pp. 1391–1395, 2002.